A finite element method for the two-dimensional extended Boussinesq equations

Mark Walkley*,† and Martin Berzins

Computational PDE Unit, School of Computing, University of Leeds, Leeds LS2 9JT, U.K.

SUMMARY

A new numerical method for Nwogu's (*ASCE Journal of Waterway, Port, Coastal and Ocean Engineering* 1993; **119**:618) two-dimensional extended Boussinesq equations is presented using a linear triangular finite element spatial discretization coupled with a sophisticated adaptive time integration package. The authors have previously presented a finite element method for the one-dimensional form of these equations (M. Walkley and M. Berzins (*International Journal for Numerical Methods in Fluids* 1999; **29**(2):143)) and this paper describes the extension of these ideas to the two-dimensional equations and the application of the method to complex geometries using unstructured triangular grids. Computational results are presented for two standard test problems and a realistic harbour model. Copyright © 2002 John Wiley & Sons, Ltd.

KEY WORDS: extended Boussinesq equations; finite element method; adaptive time integration

1. INTRODUCTION

Boussinesq equations model weakly non-linear, weakly dispersive water waves in a variable depth environment; in shallow water their linearized dispersion characteristics approximate Stokes first-order wave theory [1]. In the nearshore zone accurate prediction of wave activity needs to account for both non-linear and dispersive effects in order to model wave processes such as diffraction, refraction, shoaling and harmonic interaction. Boussinesq models are commonly used for predicting wave elevations inside harbours [2, 3] and wave interactions in the nearshore zone [4]. All Boussinesq-type equation systems are derived by integrating the higher dimensional fluid flow equations through the depth. This produces a simplified vertical velocity distribution which restricts the validity of the mathematical model to a shallow-water environment. The original system of Boussinesq equations proposed by Peregrine [5] is

---

* Correspondence to: M. A. Walkley, Computational PDE Unit, School of Computing, University of Leeds, Leeds LS2 9JT, U.K.
† E-mail: markw@comp.leeds.ac.uk

limited to very shallow water; however, in recent years, many extended Boussinesq systems have been proposed for which the dispersion relationship is valid up to the deep water limit, increasing the useful range of these models for many applications [6–8]. In this work an extended Boussinesq system due to Nwogu [6] is used, derived from the full fluid equations by choosing the velocity at an arbitrary depth as one of the variables. Many of the extended equation systems can be shown to have equivalent linearized dispersion characteristics [7], but the proposed finite element method is easier to apply to this form of the equations for reasons given in Section 2.

The depth integration of the governing equations reduces the spatial dimension of the equations by one and makes them relatively efficient to solve numerically. Numerical schemes for one-dimensional Boussinesq equation systems were reviewed in a previous work [9] and here the attention is focused on schemes for the two-dimensional equations. Many numerical schemes for the Boussinesq equations are based on finite difference methods. Abbot et al. [2, 10] pioneered the finite difference solution of the original Boussinesq system. This scheme was probably the first Boussinesq model to be used as an engineering tool and an application to a real harbour geometry was reported in their work. Hauguel [11] and Smallman and Cooper [12] have also described finite difference schemes applied to harbour geometries. Nwogu applied a finite difference method to his extended Boussinesq system and has used it to model multi-directional wave interactions in the nearshore zone [4]. Wei and Kirby [13] described a different finite difference model of Nwogu's equations and this method has subsequently been used by Zang et al. [14] and Skotner and Apelt [15] for prototype harbour geometries. Schröter et al. [16] applied a finite difference method, similar in principle to that of Abbot et al., to a different set of extended Boussinesq equations and this model was used to simulate the wave disturbances in a real harbour geometry, reported in a separate publication [3]. The finite difference methods are simple to formulate, but difficulties in modelling irregular geometries in two space dimensions with structured grids can lead to a loss of accuracy [3]. More recent work has investigated the use of boundary-fitted grids which go some way to addressing this problem [17, 18]; however, the accuracy can be limited by the need for an orthogonal grid, and considerable work may be needed to generate such a grid for an arbitrary geometry. Unstructured finite element methods are straightforward to apply on complex domains but their application in this area has mainly been limited to the original Boussinesq system and structured grids [19, 20]. Kawahara et al. [21, 22] have applied a linear finite element method to the equations, including the use of a fully unstructured mesh to analyse the wave elevations in a real bay. Ambrosi et al. [23] applied a linear triangular Taylor–Galerkin finite element method to simulate the wave elevation past a cylindrical obstacle. Langtangen et al. [24] described linear and quadratic finite element methods within the framework of the DIFFPACK software and applied them to model problems on unstructured meshes. There is little published material on the application of finite element methods to extended Boussinesq equations. The authors' previous work [9] described a finite element method for Nwogu's one-dimensional extended Boussinesq equations and more recently Li et al. [25] have described a linear quadrilateral finite element method for a different set of extended Boussinesq equations, due to Beji and Nadaoka [7]. Woo and Liu [26] have recently described a Petrov–Galerkin finite element method for one-dimensional fully non-linear, weakly dispersive wave equations which are structurally very similar to the equations considered here. These methods have some similarities with that presented here and the approaches are compared and contrasted throughout this work.

In this work, a method of lines approach is adopted. A complete spatial discretization is performed producing a system of ordinary differential equations in time, and boundary conditions in either algebraic or differential form. This differential–algebraic equation system is solved using DASPK [27]; a general purpose time integration package using adaptive order, adaptive time stepping methods driven by state-of-the-art local error control strategies. The aim of this work is to investigate the application of the finite element method to geometrically complex two-dimensional problems using unstructured triangular meshes. However, the linear Galerkin finite element method cannot be applied directly to the system due to the presence of third-order spatial derivatives. Here, the equations are rewritten in a lower order form suitable for a linear finite element approximation by introducing auxiliary algebraic equations. The additional computational expense of solving these equations is reduced by approximating them in an explicit form.

The remainder of this paper is structured as follows. Section 2 describes the chosen mathematical model for shallow water flow and shows the derivation of the modified form of the equations used in this work. Section 3 describes the numerical method; a linear triangular finite element method for the spatial approximation coupled with a sophisticated adaptive time integration strategy. Particular attention is paid to the boundary conditions, and a new formulation of the wall boundary condition is presented here. Initial conditions are presented that allow efficient use of the adaptive time integration strategy. In Section 4, numerical experiments are presented comparing the proposed method with experimental data and applying the method to a prototype harbour geometry. Issues concerned with the specification of the incident wave are considered and a method is proposed and demonstrated numerically. Section 5 discusses the results and considers the issues involved in using the model as an engineering design tool.

2. THE BOUSSINESQ EQUATION SYSTEM

The physical system can be characterized by a typical water depth H, a typical wavelength λ and a typical wave amplitude a. The non-linearity and dispersion present in the system are parameterized by the ratios ε and σ, respectively. Ursell [28] discovered a correlation between these two parameters that predicts which wave theory will be applicable. This is known as the Ursell Number, U. In terms of H, λ and a the values of ε, σ and U are given by

$$\varepsilon = \frac{a}{H}, \quad \sigma = \frac{H}{\lambda}, \quad U = \frac{\varepsilon}{\sigma^2} = \frac{a\lambda^2}{H^3} \tag{1}$$

The Boussinesq wave theory requires $\varepsilon \ll 1$, $\sigma \ll 1$ and U to be $\mathcal{O}(1)$. The equation system can then be consistently derived from the inviscid, incompressible, irrotational fluid flow equations by suitably scaling and non-dimensionalizing the equations, integrating through the depth and then expanding in terms of the small parameters σ and ε [6]. Terms up to and including $\mathcal{O}(\varepsilon, \sigma^2)$ are retained.

Nwogu's extended Boussinesq equation system is given below in terms of the free surface elevation $\eta(x, y, t)$, horizontal velocity field $\mathbf{u}(x, y, t) = (u(x, y, t), v(x, y, t))$ at depth $z = \theta h$ and spatially varying depth $h(x, y)$ with respect to a horizontal co-ordinate

system (x, y).

$$\frac{\partial \eta}{\partial t} + \nabla \cdot ((h + \eta)\mathbf{u}) + \nabla \cdot (A_1 h^3 \nabla(\nabla \cdot \mathbf{u}) + A_2 h^2 \nabla(\nabla \cdot (h\mathbf{u}))) = 0 \qquad (2)$$

$$\frac{\partial \mathbf{u}}{\partial t} + g\nabla \eta + (\mathbf{u} \cdot \nabla)\mathbf{u} + B_1 h^2 \nabla \left(\nabla \cdot \frac{\partial \mathbf{u}}{\partial t} \right) + B_2 h \nabla \left(\nabla \cdot \left(h \frac{\partial \mathbf{u}}{\partial t} \right) \right) = 0 \qquad (3)$$

where

$$A_1 = \frac{\theta^2}{2} - \frac{1}{6}, \qquad A_2 = \theta + \tfrac{1}{2}, \qquad B_1 = \frac{\theta^2}{2}, \qquad B_2 = \theta \qquad (4)$$

and ∇ represents the two-dimensional vector differential operator with respect to the horizontal co-ordinates (x, y). The free parameter $\theta = z/h$ is chosen to minimize the difference between the equations' linearized dispersion characteristics and the full linear dispersion relation. A more detailed discussion of this choice is given in References [6, 13]. The value $\theta = -0.531$, suggested by Nwogu [6], is used throughout this work.

Equation (2) contains third spatial derivatives and, if a standard linear triangular finite element method is to be applied to this system, must be modified into a form containing at most second spatial derivatives. In one dimension the authors introduced one auxiliary equation into the system to remove the third spatial derivatives [9] and this approach is extended here to the two-dimensional system. The structure of Equation (2) suggests the definition of a vector $\mathbf{w}$;

$$\mathbf{w} = A_1 h^3 \nabla(\nabla \cdot \mathbf{u}) + A_2 h^2 \nabla(\nabla \cdot (h\mathbf{u})) \qquad (5)$$

This will introduce two additional differential equations into the system, but admits a linear triangular spatial approximation. Note that Li *et al*. [25] modify the extended equation system of Beji and Nadaoka in a similar way by defining the gradient of the free surface elevation as an auxiliary variable. The Petrov–Galerkin finite element method of Woo and Liu [26] has no such restriction: C^2 cubic spline weight functions are used allowing a direct approximation of the third space derivatives. However, while possible on mildly unstructured quadrilateral grids in two dimensions, this method may prove too complicated to apply on arbitrary grids and geometries.

The equation system is further modified by approximating the convection terms in momentum equation (3)

$$(\mathbf{u} \cdot \nabla)\mathbf{u} + g\nabla \eta = \nabla(\tfrac{1}{2}|\mathbf{u}|^2 + g\eta) + \mathcal{O}(\sigma^2) \qquad (6)$$

which is an acceptable approximation within the Boussinesq framework [29].

Using these results in equation system (2)–(3) gives the system of equations to be solved here:

$$\frac{\partial \eta}{\partial t} + \nabla \cdot \mathbf{p} + \nabla \cdot \mathbf{w} = 0 \qquad (7)$$

$$\frac{\partial \mathbf{u}}{\partial t} + \nabla f + B_1 h^2 \nabla \left(\nabla \cdot \frac{\partial \mathbf{u}}{\partial t} \right) + B_2 h \nabla \left(\nabla \cdot \left(h \frac{\partial \mathbf{u}}{\partial t} \right) \right) = 0 \qquad (8)$$

$$\mathbf{w} - A_1 h^3 \nabla(\nabla \cdot \mathbf{u}) - A_2 h^2 \nabla(\nabla \cdot (h\mathbf{u})) = 0 \qquad (9)$$

where

$$\mathbf{p} = (h + \eta)\mathbf{u}, \quad f = \tfrac{1}{2}|\mathbf{u}|^2 + g\eta \tag{10}$$

3. THE NUMERICAL METHOD

3.1. Spatial discretization

The two-dimensional finite element method is developed by partitioning the spatial domain Ω into a set of *ne* non-overlapping triangular elements that completely cover the domain. A piecewise linear interpolation can be defined over this set of triangular elements by using the common vertices to define a set of *np* nodes. A set of *np* linear global basis functions $\phi_i(x, y)$ are then defined on the set of nodes

$$\phi_i(x_j, y_j) = \delta_{ij} \tag{11}$$

where δ_{ij} is the Dirac delta function.

For simplicity of presentation a constant depth H is assumed initially. The extension to a variable depth $h(x, y)$ is considered afterwards. Discretizing equation system (7)–(9), with $\dot{\psi}_j$ denoting the time derivative of ψ_j,

$$\mathbf{M}_{ij}\,\dot{\eta}_j + \mathbf{C}_{ij}^m\,p_j^m + \mathbf{C}_{ij}^m w_j^m = 0 \tag{12}$$

$$\mathbf{M}_{ij}\,\dot{u}_j^m + \mathbf{C}_{ij}^m f_j - (B_1 + B_2)H^2\mathbf{K}_{ij}^{mn}\,\dot{u}_j^n = -(B_1 + B_2)H^2\int_{\Gamma} \phi_i\nabla\cdot\,\dot{\mathbf{u}}\,\hat{n}^m\,\mathrm{d}\Gamma \tag{13}$$

$$\mathbf{M}_{ij}w_j^m + (A_1 + A_2)H^3\mathbf{K}_{ij}^{mn}u_j^n = (A_1 + A_2)H^3\int_{\Gamma} \phi_i\nabla\cdot\mathbf{u}\,\hat{n}^m\,\mathrm{d}\Gamma \tag{14}$$

where Γ denoted the boundary of Ω, $\hat{\mathbf{n}} = (\hat{n}^1, \hat{n}^2)$ is the unit outward normal on the boundary, and

$$\mathbf{M}_{ij} = \int_{\Omega} \phi_i\phi_j\,\mathrm{d}\Omega, \quad \mathbf{C}_{ij}^m = \int_{\Omega} \phi_i\frac{\partial\phi_j}{\partial x_m}\,\mathrm{d}\Omega, \quad \mathbf{K}_{ij}^{mn} = \int_{\Omega} \frac{\partial\phi_i}{\partial x_m}\frac{\partial\phi_j}{\partial x_n}\,\mathrm{d}\Omega \tag{15}$$

with $(x_1, x_2) \equiv (x, y)$. Summation over the repeated indices is implied.

The non-linear terms $\mathbf{p}$ and f are approximated in a compact form by direct interpolation with the basis functions. In one dimension this was found to lead to a more accurate discretization [9].

The extension to the variable depth system (7)–(9) is shown by considering a single term from Equation (9), with the other dispersive terms discretized in a similar manner.

$$\int_{\Omega} \phi_i A_2 h^2\nabla(\nabla\cdot(h\mathbf{u}))\,\mathrm{d}\Omega = -A_2\int_{\Omega} \nabla(\phi_i h^2)\nabla\cdot(h\mathbf{u})\,\mathrm{d}\Omega + A_2\int_{\Gamma} \phi_i h^2\nabla\cdot(h\mathbf{u})\,\hat{\mathbf{n}}\,\mathrm{d}\Gamma$$

$$= -A_2\int_{\Omega} (\phi_i\nabla(h^2) + h^2\nabla\phi_i)\nabla\cdot(h\mathbf{u})\,\mathrm{d}\Omega$$

$$+ A_2\int_{\Gamma} \phi_i h^2\nabla\cdot(h\mathbf{u})\,\hat{\mathbf{n}}\,\mathrm{d}\Gamma. \tag{16}$$

The h^2 and $h\mathbf{u}$ terms are approximated by direct linear interpolation of the products, a strategy that proved effective in the one-dimensional scheme [9]. The other dispersive terms in Equations (13) and (14) are approximated in a similar manner. Li *et al.* [25] neglect certain terms from the variable depth equations and hence, their underlying mathematical model may be slightly less accurate at this point.

Here, the auxiliary equation (14) is approximated in an explicit form by *lumping* [30] the mass matrix, $\mathbf{M}_{ij}$, which allows direct calculation of the $\mathbf{w}_j$. In one dimension, it was shown that this did not decrease the accuracy of the discretization significantly [9] and the computational cost is significantly reduced in this case since $\mathbf{M}_{ij}$ will be a sparse matrix in general. The $\mathbf{w}_j$ coefficients are computed prior to the assembly of the time-differential equations which reduces the number of unknowns at a node from 5 to 3 in the final assembled system. This will make the scheme competitive with existing finite difference schemes which can directly approximate the third spatial derivatives without the introduction of auxiliary equations.

For the numerical examples considered here three boundary conditions are required; inflow, outflow and solid wall conditions. Inflow boundary conditions are imposed in Dirichlet form from a given distribution, in this case a sinusoidal form for the free surface $\eta_{\text{in}}(t)$. The velocity $\mathbf{u}_{\text{in}}(t)$ and the auxiliary variable $\mathbf{w}_{\text{in}}(t)$ are computed from a linearized approximation to the equation system [29] which is accurate if the depth at the inflow boundary is sufficiently large, i.e. $\varepsilon \ll 1$. This condition will generally be appropriate for the type of problem considered here, where waves are propagated from deep water towards a structure near the shore. If non-linearity is significant, corrections can be derived which include the first-order effects of non-linearity on the sinusoidal distribution [29]. Outflow boundary conditions are required to remove waves from the simulation that approach open boundaries. Here the standard technique of viscous damping is used, termed *sponge layers* [31]. A viscous term is added to the free surface equation, the coefficient zero in most of the domain and increasing exponentially as it approaches the outflow boundary. The precise choice is determined by experiment; here the coefficient is chosen so as to be non-zero for a distance of approximately two wavelengths. In one dimension, this approach is effective at removing waves without significant non-physical reflection [29]; however, in two dimensions it can be less effective, particularly for waves approaching at oblique angles. Solid walls are treated as impermeable in the problems considered here and the starting point is the condition

$$\mathbf{u}\cdot\mathbf{n} = 0 \tag{17}$$

on the velocity. Additional boundary conditions are required to close the system at the boundary, the first of which is derived from a conservation of mass argument. Integrating the free surface equation (7) over the domain and applying the divergence theorem

$$\frac{\partial}{\partial t} \int_{\Omega} \eta \, \mathrm{d}\Omega + \int_{\Gamma} (\mathbf{p} + \mathbf{w})\cdot\mathbf{n} \, \mathrm{d}\Gamma = 0. \tag{18}$$

At the solid wall there is no loss of mass, hence the first term is zero, and condition (17) and the definition of $\mathbf{p}$ (10) imply $\mathbf{p}\cdot\mathbf{n} = 0$. Condition (18) is, therefore, satisfied by the additional constraint

$$\mathbf{w}\cdot\mathbf{n} = 0 \tag{19}$$

The system is closed by deriving tangential evolution equations for the velocity and auxiliary variable, formed by taking the dot product of the vector equations (8) and (9) with the tangent vector at the wall, noting that the boundary integrals produced during the spatial discretization process vanish in both cases [29]. This approach is similar, in principle, to that presented by Engelman *et al.* [32] for incompressible flow. In previous work, the wall boundary condition (17) has been supplemented with heuristic conditions on the velocity gradient [13, 25], at the expense of evolutionary equations for the variables there; however, the formulation here requires no such assumptions.

In the numerical results presented in the following section, there is some evidence of high-frequency oscillations over the mesh. Similar effects have been noted by some finite difference practitioners. Kirby *et al.* [33] report using numerical filtering (averaging) every four wave periods to remove high-frequency errors. Schröter *et al.* [3] remove high-frequency 'noise' by either local or global '*spatial smoothing*'. In an attempt to remedy this, here a small amount of fourth-order viscosity is added to the free surface equation (12). It is hoped that this fourth-order derivative term will not corrupt the physical dispersion present in the system which has at most third-order spatial derivatives. The fourth-order derivative is calculated by first recovering a second derivative at the nodes of the mesh and then repeating the recovery process with these nodal values. The amount of viscosity added is manually tuned and is kept to the minimum possible, and the results indicate that this can control the oscillations without significantly damping the global solution.

3.2. Time integration

Truncation errors from a low-order time integration scheme will produce non-physical dispersion and contaminate the mathematical model. In previous work, the time integration has usually been with a high-order accuracy predictor–corrector method [13, 14], or with a lower-order method corrected for the dispersive truncation errors [6, 10]. In this work, we achieve the necessary accuracy by making use of variable order, variable time step software based on backward differentiation formulae (BDF) as implemented in the DASPK software [27].

The spatial discretization described in Section 3.1 results in a $3np$-dimensional linear system of differential equations in the form

$$\mathbf{A}_{ij} \dot{y}_j - f_i = 0 \tag{20}$$

where

$$y = (\eta_1, u_1, v_1, \eta_2, u_2, v_2, \ldots, \eta_{np}, u_{np}, v_{np})^{\mathrm{t}}, \qquad f = f(t, y) \tag{21}$$

The software controls the local error in y over each time step by varying both the order of the BDF method and the time step, so that a uniformly high accuracy in time can be achieved [34]. The user controls the local error by supplying relative and absolute tolerances, rtol and atol, respectively, which can be vector quantities in general. Here, rtol and atol are scalar values determined by experiment; lowering their values until solution independency is established. This will ensure that the error in the solution is dominated by the spatial discretization error. In this work, rtol $=$ atol $= 10^{-6}$ was chosen after repeated experiments, reflecting the high accuracy required in the time integration.

The finite element method described in the previous system will typically produce a sparse matrix system. The matrix $\mathbf{A}_{ij}$ in system (20) will, in general, also be non-positive definite,

due to the form of the dispersive terms in Equation (13), and non-symmetric, due to the imposition of the boundary conditions. Within the time integration software the non-linear system

$$\mathbf{J}_{ij}(y)\Delta y_j = -\alpha\,\Delta t\,r_i(y) \tag{22}$$

is solved at each time step, where

$$r_i = f_i - \mathbf{A}_{ij}\dot{y}_j, \qquad \mathbf{J}_{ij}(y) = \alpha\,\Delta t\,\frac{\mathrm{d}f_i}{\mathrm{d}y_j} - \mathbf{A}_{ij} \tag{23}$$

$\mathbf{J}_{ij}$ is the Jacobian matrix, α is a constant dependent on the BDF method used and Δt is the time step length. In practice, a direct solution of equation system (22) is too computationally expensive and an iterative method is employed. DASPK has been combined with the SPARSKIT software [27] and the preconditioned GMRES iterative method is used here. It is found here that simple preconditioners, such as diagonal scaling or graph-based incomplete factorizations, are inefficient and that a relatively expensive preconditioner must be used based on an incomplete lower–upper factorization of the matrix with a numerical drop tolerance strategy [35], denoted here as ILU(tol). A reverse Cuthill–McKee (RCM) algorithm [36] is also employed to reorder the nodes so as to minimize the mesh, and hence matrix, bandwidth. This is found to greatly improve the efficiency of the ILU(tol) strategy since it constrains the factorized matrix to lie within a narrower bandwidth and hence the incomplete factorization is generally more accurate for a prespecified amount of storage. Recent work by Benzi *et al.* [37] also concluded that the use of RCM was advantageous for non-symmetric matrix problems.

Consistent initial conditions are calculated automatically by the software. Given an initial solution, $y(t_0)$, initial time derivatives, $\dot{y}(t_0)$, are computed such that system (20) is satisfied [38]. Here, it is common to begin the computation with an undisturbed free surface and introduce waves gradually from the inflow boundaries in which case the initialization problem is trivially satisfied. To ensure a smooth start-up at the inflow boundary the initial wave form is modified by multiplication with a damping factor that increases from 0 to 1 over a prespecified time period [29]. This removes numerical oscillations that can occur if an undamped wave is introduced into a previously undisturbed region. A similar procedure was described by Li *et al.* [25].

3.3. Mesh generation

Unstructured triangular meshes are generally required for problems with an irregular boundary shape. Here, such meshes are produced with the Delaunay mesh generation software Triangle [39]. Problems with simple domain geometry, such as the examples considered in Sections 4.1 and 4.2, can be meshed with structured rectangular grids. This allows a fixed resolution of the expected wavelength in the model.

When unstructured triangular meshes are used it has proved beneficial to require a very smooth variation in the mesh size. In one dimension, it was shown that a variation in mesh size produced non-physical dispersion, but that this could be limited by constraining the local change in the mesh size [9]. In two dimensions, a similar procedure is possible when using structured meshes. For unstructured meshes, nodal smoothing and edge swapping operations are used to post-process the mesh and reduce the local variation in the mesh size [29]. The

application of these techniques to a harbour geometry is described in Section 4.3. It is also found that the model can be sensitive to the orientation of the diagonal edges in a structured triangular mesh, and that the best results are obtained if diagonals alternate, producing a symmetric nodal stencil at each mesh point [29].

4. NUMERICAL EXPERIMENTS

In this section two model problems and a more realistic harbour problem are used to illustrate the performance of the method.

4.1. Wave focusing by a topographic lens

This variable depth case is a standard test for dispersive wave models [7, 8, 14, 25]. The semicircular ramp focuses the waves behind the slope causing a large increase in wave height in the centre of the channel and a corresponding decrease at the edges. An accurate model of wave refraction is required to predict the correct position of the peak wave height.

The domain is $(x, y) \in [0, 6.096] \times [0, 35]$ with an inflow boundary at $y = 0$ and solid walls at $x = 0$ and 6.096. The outflow boundary at $y = 35$ has an absorbing sponge layer, active for $y \in [32, 35]$. The depth variation within the domain is given by

$$g_x = (6.096x - x^2)^{1/2}$$

$$h(x, y) = \begin{cases} 0.4572 & y \leqslant 10.67 - g_x \\ 0.4572 + 0.04(10.67 - g_x - y) & 10.67 - g_x < y < 18.29 - g_x \\ 0.1524 & y \geqslant 18.29 - g_x \end{cases}$$

and is shown in Figure 1.

The inflow wave is of the form

$$\eta_{\text{in}} = \sin\left(2\pi\left(\frac{y_{\text{in}}}{\lambda} - \frac{t}{\tau}\right)\right) \tag{24}$$

where the wave amplitude a, period τ and wavelength λ are

$$a = 0.0195\,\text{m}, \qquad \tau = 1.0\,\text{s}, \qquad \lambda = 1.488\,\text{m} \tag{25}$$

A mesh resolution of 0.1 m, approximately 15 points per wavelength, is used throughout the domain.

Figure 2 shows the free surface elevation profile on three lengthwise sections of the channel, $x = \{1.016, 2.032, 3.048\,\text{m}\}$, at time $t = 40$ s by which time a steady periodic flow has been established. The maximum and minimum wave elevations obtained visually match those taken from the wave envelope and centreline plots of Madsen and Sørensen [8].

4.2. Wave propagation over an elliptical shoal

This test problem has been reported in several studies of extended Boussinesq equations [13, 14] and experimental data is available in the form of wave height coefficient

(a) Depth contours on the mesh

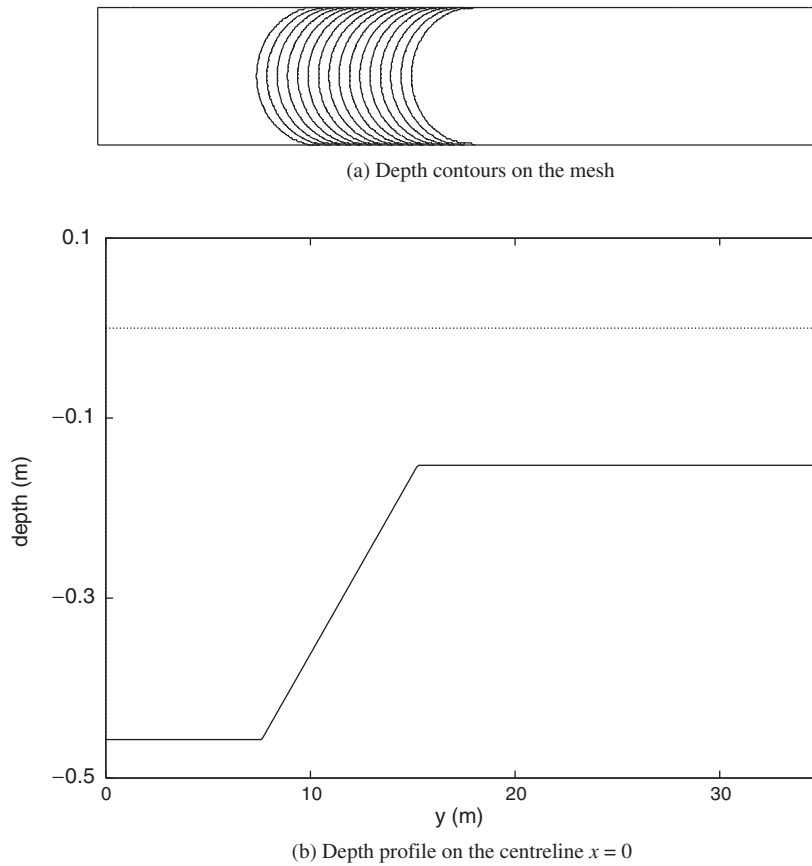(b) Depth profile on the centreline $x = 0$

Figure 1. Spatial depth profile for the wave focusing experiment.

measurements, which represent the maximum wave height at a point, taken over several wave periods, normalized with the inflow wave height. A complex periodic wave field is established over the domain due to interactions produced by waves refracted by the varying slope.

The domain is $(x, y) \in [-10, 10] \times [-15, 10]$ with an inflow boundary at $y = -15$ and solid walls at $x = 10$ and -10. The outflow boundary at $y = 10$ has an absorbing sponge layer, active for $y \in [7, 10]$.

The depth variation within the domain is given by a combination of a $1:50$ slope at an angle of $20°$ to the y-axis

$$x_r = \cos(20) x - \sin(20) y, \qquad y_r = \sin(20) x + \cos(20) y,$$

$$h(x, y) = \begin{cases} 0.45 & y_r \leqslant -5.82, \\ 0.45 - 0.02(5.82 + y_r) & y_r > -5.82, \end{cases}$$
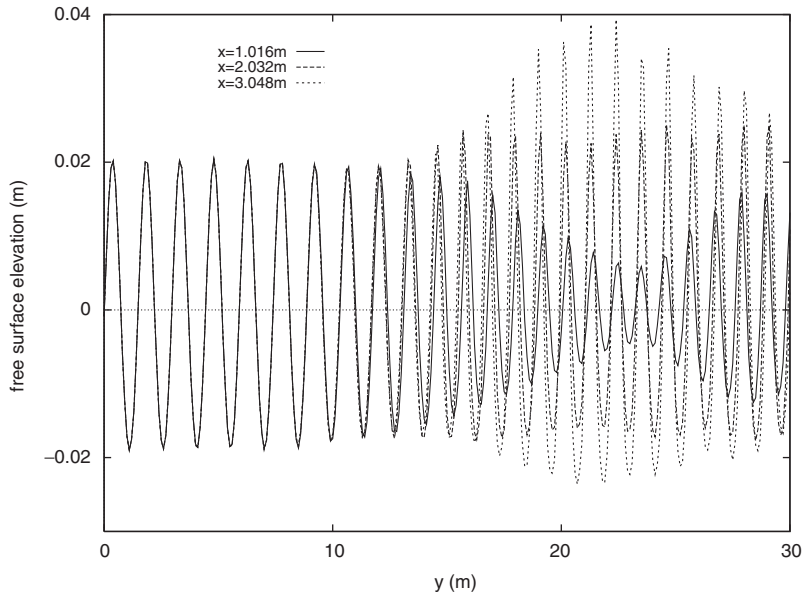
Figure 2. Wave focusing experiment: lengthwise free surface elevations at $t = 40$ s.

up to a minimum depth of 0.1 m, and an elliptical bump centred on the origin. For the region

$$\left(\frac{x_{\mathrm{r}}}{4}\right)^2 + \left(\frac{y_{\mathrm{r}}}{3}\right)^2 < 1$$

the depth is modified by

$$h(x, y) \Rightarrow h(x, y) + 0.3 - \frac{1}{2}\left(1 - \left(\frac{x_{\mathrm{r}}}{5}\right)^2 - \left(\frac{y_{\mathrm{r}}}{3.75}\right)^2\right)^{1/2}$$

The depth profile is shown in Figure 3.

The inflow wave is of the form (24) with parameters

$$a = 0.0232 \text{ m}, \qquad \tau = 1.0 \text{ s}, \qquad \lambda = 1.485 \text{ m} \tag{26}$$

and a mesh resolution of 0.1 m, approximately 15 points per wavelength, is used throughout the domain.

Experimental data is available in the form of wave height coefficient measurements on the following co-ordinate sections:

$$\{(x, y_{\mathrm{m}}),\ y_{\mathrm{m}} = 1.0, 3.0, 5.0, 7.0, 9.0\}, \qquad \{(x_{\mathrm{m}}, y),\ x_{\mathrm{m}} = -2.0, 0.0, 2.0\} \tag{27}$$

The measurements are taken over the time period [42, 44] by which time the waves are progressing steadily across the domain.

Figure 4 shows the plots of wave height coefficient for the numerical scheme and also for the experimental data from the original laboratory experiment. Comparison of these results with those previously published shows a much better agreement with the experimental data.

(a) Depth contours on the mesh

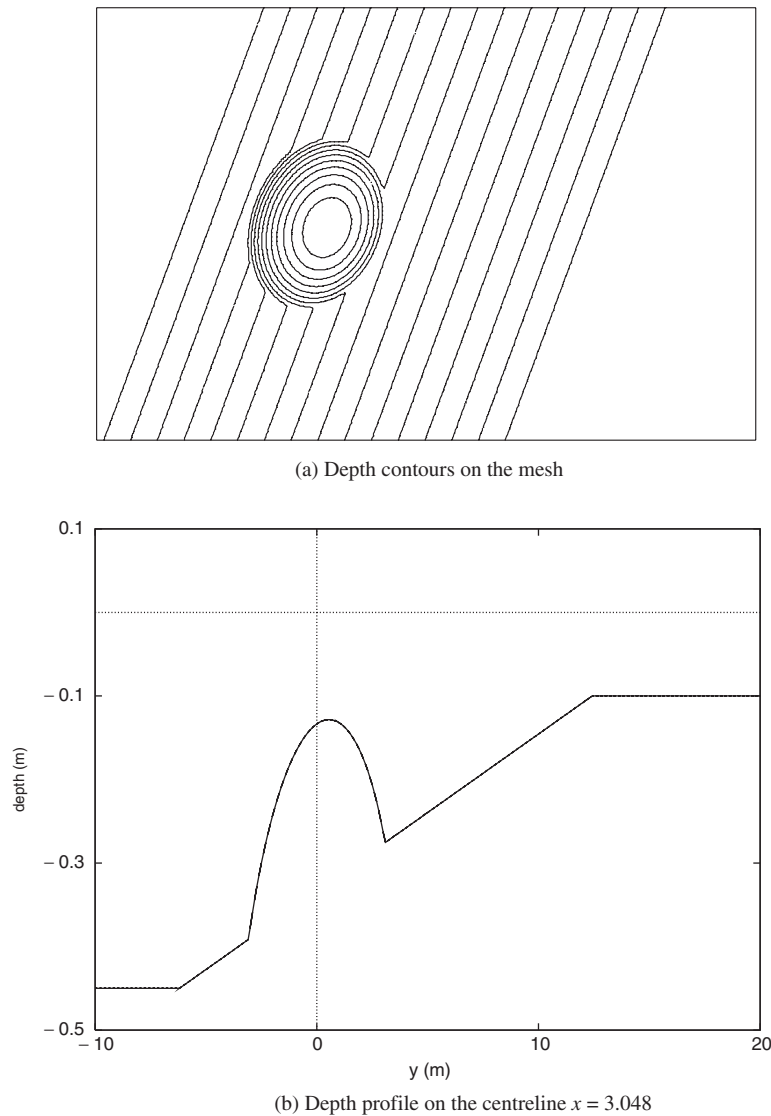(b) Depth profile on the centreline $x = 3.048$

Figure 3. Spatial depth profile for the elliptical shoal experiment.

Wei and Kirby's finite difference method [13] predicts a wider central focusing region in Figures 4(c)–4(e) and does not capture the secondary peaks very accurately. Their results for the sections shown in Figures 4(f) and 4(h) show large differences near $y = 10$ and also a large deviation from the experimental data on the section shown in Figure 4(g) in a region just behind the elliptical bump. The results of Zang *et al.* [14] produced with a similar finite difference scheme show an improved model of the central focusing regions in Figures 4(c)–4(e) but a relatively poor representation of the secondary peaks on those sections. Their
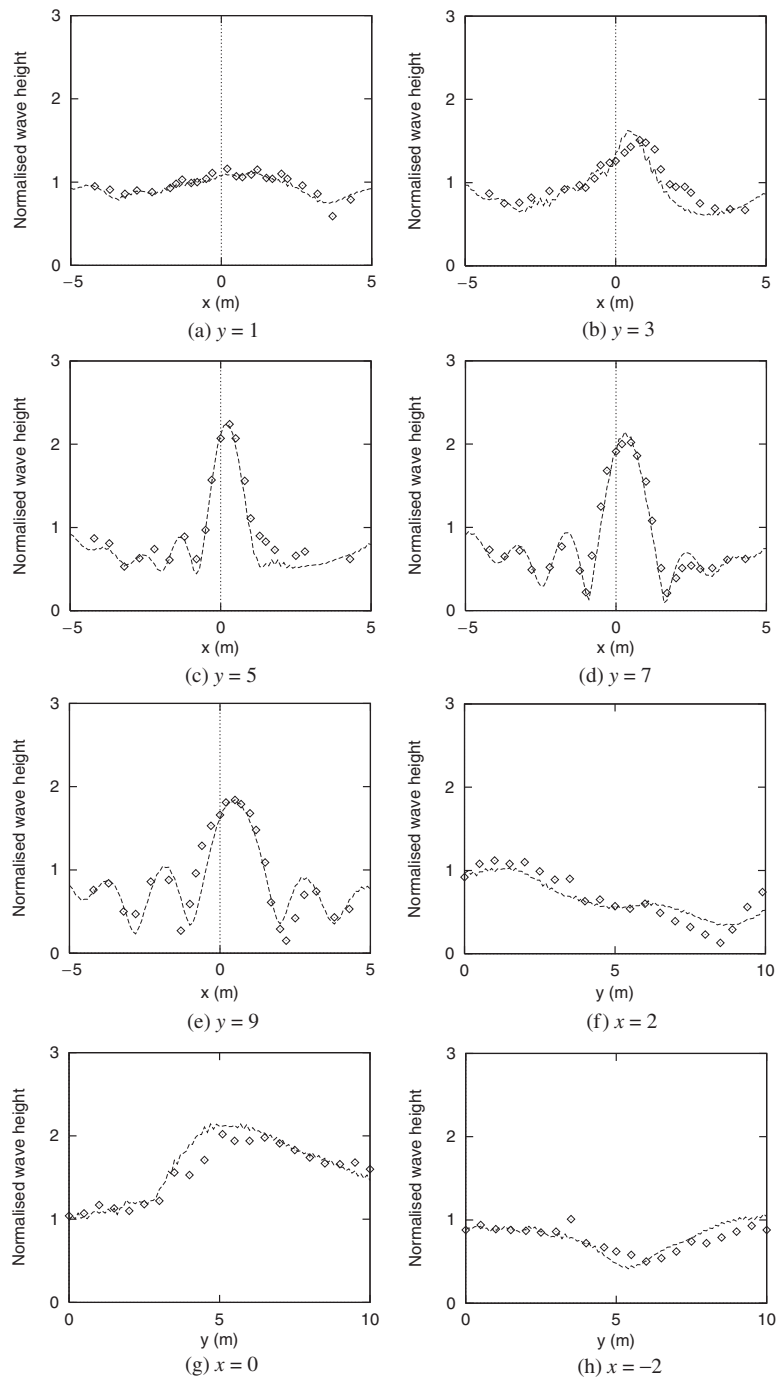
Figure 4. Wave height coefficient sections for the elliptical shoal experiment.
(line—numerical. data points—experimental).

results for the section shown in Figure 4(g) appear more accurate than Wei and Kirby's although the two other lengthwise sections are not shown in that work. The mesh resolutions used in these two works are not, however, specified. In a more recent publication, Wei *et al.* [40] have solved this problem again using the same finite difference scheme with an internal wave-generation method for the incident wave. A mesh resolution of 0.05 m, approximately 30 points per wavelength, is used here. These results are very similar to those presented here although they do not appear to have any oscillations in their data. However, they note that the results are calculated by averaging the results over four wave periods which may remove such high-frequency noise.

### 4.3. A prototype harbour geometry

The motivation for this work was to model the wave disturbance inside and around harbours. Previously published studies using finite difference models were reviewed in Section 1. To the author's knowledge there have been no finite element Boussinesq models applied to such problems.

The model considered here is based on a HR Wallingford case study of a real harbour [41]. The exact geometry data supplied with the case study is shown as the solid boundary on Figure 5(a). The computational domain used is fully specified by introducing additional seaward boundaries as shown in the figure. These are chosen to be suitably far from the region of interest, but are constrained by the expected size of the finite element grid which must not be too large for practical computations. The mesh generation procedure adopted is to generate a coarse unstructured grid, suitable for representing the geometry, and then to post-process the mesh by successively applying coordinate smoothing and edge swapping to produce a reasonably smooth variation in the mesh size. The mesh is then uniformly subdivided to produce a finer grid and that grid is then post-processed with the same procedures. This is repeated until a suitable mesh size is reached; in this case, a resolution of the expected inflow wave of approximately 20 nodes per wavelength. Figure 5(b) shows an intermediate mesh produced by the post-processing after three levels of uniform refinement. Note that the boundary definition shown in Figure 5(a), taken from the report, is modified slightly by prescribing a finite thickness to the boundary regions. A similar procedure is carried out for the HR Wallingford case study although the exact dimensions will not be identical. In the computational model used here all physical boundaries are assumed to be vertical and perfectly reflecting, although this was not the case in reality [41]. The final mesh produced contained 167 936 elements and 85 057 nodes with a resolution at the inflow boundary of approximately 24 points per wavelength. The mesh bandwidth was reduced to 350 by the Reverse Cuthill–McKee algorithm.

A constant depth is assumed over the whole region and a simple monochromatic waveform is input as the lower boundary. The flow parameters are

$$h_{\text{in}} = 7.0 \, \text{m}, \qquad a = 1.0 \, \text{m}, \qquad \tau = 5.3 \, \text{s}, \qquad \lambda = 36.5 \, \text{m} \qquad (28)$$

where the wavelength λ has been calculated to be consistent with the linear dispersion relation at the inflow boundary. The inflow wave is specified at $y = 0$ for $x \in [220, 420]$. Sponge layers are used to remove any outgoing waves at the sides of the domain $x \in [140, 220]$ and $x \in [420, 490]$. The inflow wave is specified so as not to be active inside the sponge layer regions by smoothly decreasing the wave amplitude to zero as it approaches either layer.
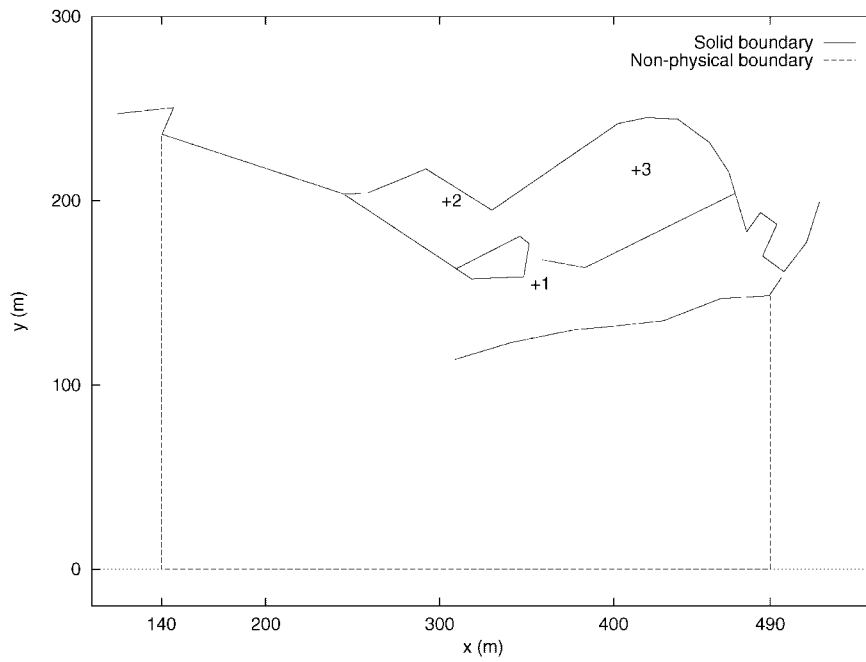
(a) Spatial domain for the harbour geometry
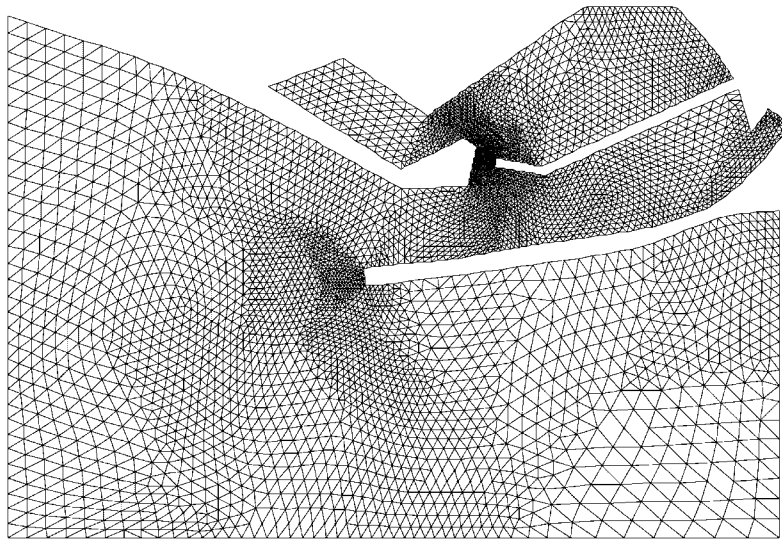
(b) Intermediate mesh generated by the post-processing

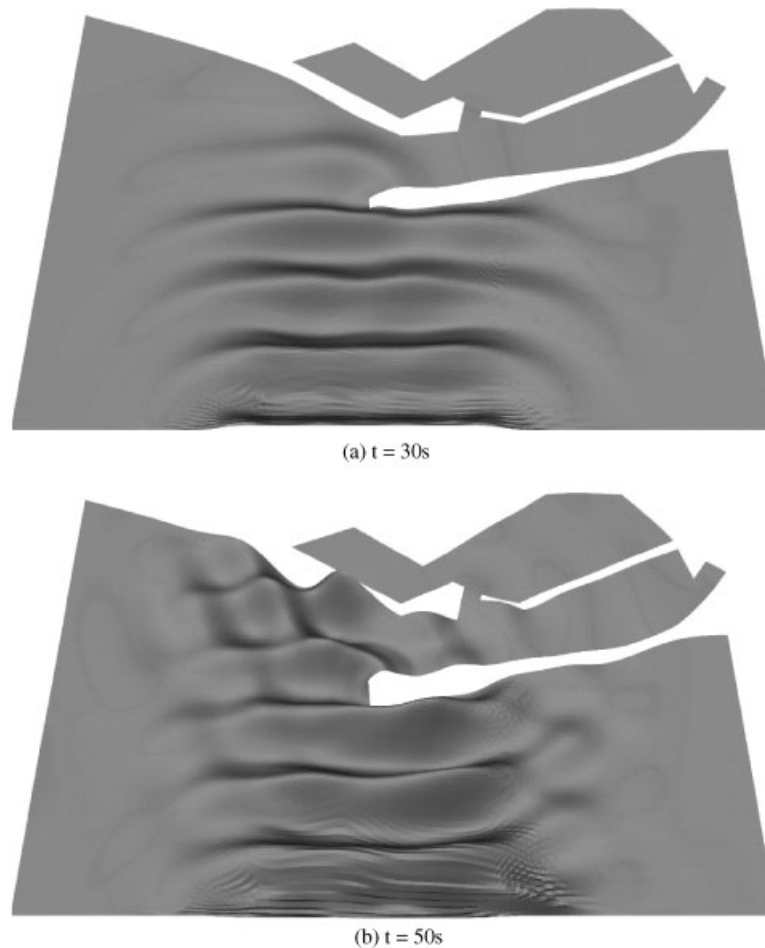Figure 5. Unstructured triangular meshes for the harbour geometry.

(a) t = 30s

(b) t = 50s

Figure 6. Perspective view of the free surface.

Figure 6 shows views of the free surface at $t = 30$ and 50 s. The waves can be seen approaching the structure and diffracting round the breakwaters and entering the harbour. However, the simulation cannot be run far enough for a steady state to be established due to the restrictions of the inflow boundary conditions. Waves reflected from the primary breakwater impinge on the inflow boundary region and since these boundaries are subject to Dirichlet conditions, they cannot leave and reflect back into the computational domain. This leads to spurious waveforms at the inflow boundary which are eventually transported into the harbour region.

4.4. Non-reflecting inflow boundary conditions

The simulation of realistic problems requires long-time calculations in order to allow the initial transient effects to be removed. If wave generation is implemented by prescribing the

waveform at the boundary, as described in the previous section, then a wave that is reflected back to that boundary will not be able to pass through that region and leave the domain. In geometrically complicated regions, interactions with solid boundaries will generally produce a multidirectional wave field and problems at such inflow boundaries will become increasingly likely.

An alternative approach is to prescribe the required wave field internally to the domain and then treat all open boundaries as outflow, which can then be bounded with sponge layers that can absorb all outgoing waves. The only requirement is that the wave generation regions be transparent to outgoing waves. Larsen and Dancy [42] were the first to describe such an approach for a two-dimensional finite difference model of the original Boussinesq equation system. They introduced an increment to the free surface along a generation line which varied periodically to produce a wave motion. They showed that this approach could be used on fairly general geometries, within the restrictions of the Cartesian finite difference grid. Skotner and Apelt [15] have described an alternative internal wave generation method for a two-dimensional finite difference model of Nwogu's extended Boussinesq equations. The method is relatively complex, involving a modified stencil in the wave generation region and explicit removal of the wave in the region behind the wave generator to prevent reflection. More recently, Wei *et al*. [40] have rigorously derived a source function that can be added to the free surface equation to generate regular or irregular wave fields inside the domain. This was implemented as part of their finite difference model for Nwogu's extended Boussinesq equations.

In one dimension, a method of generating waves internally to the domain by simulating an oscillation of the sea bed has been developed and combined with the author's one-dimensional Boussinesq model [29]. An analogy is drawn with a time-varying sea bed, and a term is added to the free surface equation that simulates the lowest order effects of a time varying depth profile. In the free surface equation (7) this takes the form

$$\dot{\eta} + \dot{h}_I + \nabla \cdot \mathbf{p} + \nabla \cdot \mathbf{w} = 0 \tag{29}$$

where the form of the sea bed variation h_I is taken to be

$$\dot{h}_I(x,t) = c_I f_I(x) a \sin(-\omega t) \tag{30}$$

and a and ω are the amplitude and frequency of the required wave, respectively, and the constant c_I and spatial function $f_I(x)$ are given by,

$$c_I = 2\omega c, \qquad f_I(x) = \frac{b_I}{\sqrt{\pi}} e^{-b_I^2(x-x_I)^2} \tag{31}$$

This simulates an undulating Gaussian hill at the position $x = x_I$. The width of this region $[x_I - a_I, x_I + a_I]$ is generally taken to be one or two wavelengths, which is consistent with the scaling of the equation system which requires variations in the depth to be small over distances comparable to the wavelength [5]. The coefficient b_I is chosen such that the function $f_I(x)$ is effectively zero at $x = x_I \pm a_I$ which is essential for the depth variation to appear smooth to the time integration software. The function $f_I(x)$ is normalized such that its integral is one over this region. The constant c_I includes a factor 2 as the wave generator will produce both a left- and right-moving wave, the wave speed c to give the expression the correct physical dimensions, and the wave frequency ω to compensate for differentiation with respect

to time. It was shown that in one dimension, it allowed reflected waves to pass through the
generation region and leave the domain. The formulation of this method produces a scheme
similar in principle to that of Wei *et al.* [40] although their wave form is more general
and they rigorously derive the necessary parameters which are empirically tuned in this case.
The time variation of the depth will also affect the dispersive terms in the system. However,
since the width of the generating region is proportional to the wavelength and the amplitude
of undulation is proportional to the wave amplitude, it is reasonable to assume that the
perturbation to the dispersive terms can be neglected within the order of approximation of the
Boussinesq system.

For complex problems, it is important that these wave generation regions can be placed
in open regions of water, without necessarily terminating at solid boundaries. In the fol-
lowing example, a wave generator is placed inside an open square region, completely sur-
rounded by damping sponge layers. The spatial domain is $(x, y) \in [-14, 14] \times [-14, 14]$ and
the wave generation function is centred on $y = 0$ with a width of approximately two wave-
lengths, and active for $x \in [-6, 6]$. All boundaries are considered to be of outflow type and
a sponge layer region is specified for $x > 10$, $x < -10$, $y > 10$ and $y < -10$. The wave
generation function is smoothly reduced to zero in the regions $x \in [-8, -6]$ and $x \in [6, 8]$.
This ensures that the wave generation is not active inside the sponge layer boundary
region.

The flow parameters are

$$h = 0.8 \, \text{m}, \qquad a = 0.01 \, \text{m}, \qquad \tau = 1.14 \, \text{s}, \qquad \lambda = 2.0 \, \text{m}$$

with the period τ calculated to satisfy the linear dispersion relation. The problem is inte-
grated in time for $t \in [0, 20]$. Figures 7(a) and 7(b) show the computed solution at $t = 20$ s.
The wave fronts in Figure 7(b) show that the generation region produces a periodic wave;
however, the contours in Figure 7(a) show that this primary wave field is contaminated
with a secondary field that appears to radiate from the ends of the generation region. Var-
ious functions can be used to specify the end regions but it has so far proved to be im-
possible to eliminate these two-dimensional end effects from the simulation and the ef-
fective, accurate use of this wave generation method is an unresolved problem at
present.

5. CONCLUSIONS AND FURTHER WORK

A new numerical method for the two-dimensional extended Boussinesq equations has been
presented combining an unstructured triangular finite element method with an adaptive time
integration package. The equation system has been rewritten in a novel form allowing a linear
spatial approximation and new boundary conditions have been formulated which are consistent
with the differential–algebraic nature of the problem. Comparison for the standard test cases
with experimental data considered in Sections 4.1 and 4.2 shows that the model can accurately
represent the physical characteristics of the flow.

The simulation of a practical problem such as the wave disturbance in a harbour considered
in Section 4.3 reveals limitations in the model. More general boundary conditions are required
if realistic situations are to be modelled, such as non-vertical or porous boundaries or beaches.
In particular, a more general formulation of the inflow boundary is required which can admit

(a) Contours of free surface elevation for
one quarter of the domain
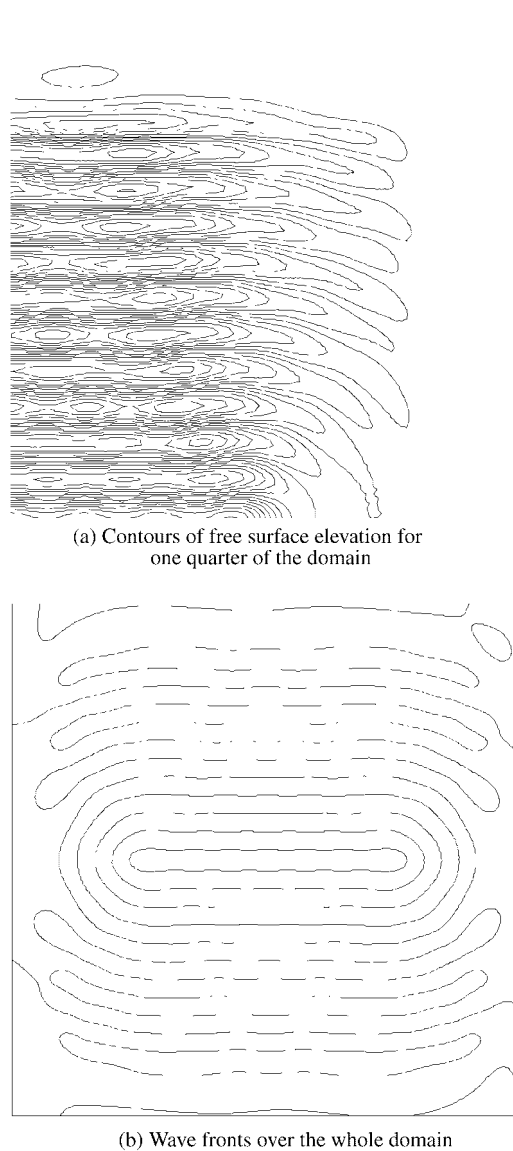

(b) Wave fronts over the whole domain

Figure 7. Spatial variation of the free surface elevation at $t = 20$ s.

multi-component, multi-directional wave forms, and also allow reflected waves to leave the domain without further non-physical reflection.

The use of non-reflecting inflow boundary conditions has been identified as crucial to the use of the model for realistic problems and work on the development of such a technique has been described in Section 4.4. This problem is currently unresolved and represents one of the main challenges in extending this model further.

REFERENCES

1. Whitham GB. *Linear and Nonlinear Waves*. Wiley/Interscience: New York, 1974.
2. Abbot MB, Petersen HM, Skovgaard O. On the numerical modelling of short waves in shallow water. *Journal of Hydraulic Research* 1978; **16**(3):173–203.
3. Schröter A, Mayerle R, Kahlfeld A, Zielke W. Assessment of a Boussinesq wave model for the design of a harbour. In *International Conference on Coastal and Port Engineering in Developing Countries*, 1995; 741–753.
4. Nwogu O. Nonlinear transformation of multi-directional waves in water of variable depth. *Draft manuscript*, 1993.
5. Peregrine DH. Long waves on a beach. *Journal of Fluid Mechanics* 1967; **27**(4):815–827.
6. Nwogu O. Alternative form of Boussinesq equations for nearshore wave propagation. *ASCE Journal of Waterway*, *Port*, *Coastal*, *and Ocean Engineering* 1993; **119**(6):618–638.
7. Beji S, Nadaoka K. A formal derivation and numerical modelling of the improved Boussinesq equations for varying depth. *Ocean Engineering* 1996; **23**(8):691–704.
8. Madsen PA, Sørensen OR. A new form of the Boussinesq equations with improved linear dispersion characteristics: Part 2. A slowly varying bathymetry. *Coastal Engineering* 1992; **18**:183–204.
9. Walkley M, Berzins M. A finite element method for the one-dimensional extended Boussinesq equations. *International Journal for Numerical Methods in Fluids* 1999; **29**(2):143–157.
10. Abbot MB, McCowan AD, Warren IR. Accuracy of short-wave numerical models. *ASCE Journal of Hydraulic Engineering* 1984; **110**(10):1287–1301.
11. Hauguel A. A numerical model of storm waves in shallow water. *Proceedings of the 17th International Conference on Coastal Engineering*, *Sydney*, *Australia*, 1980; 746–762.
12. Smallman JV, Cooper AJ. A mathematical model for set down in harbours. *Coastal Engineering* 1989; **13**: 247–261.
13. Wei G, Kirby JT. Time-dependent numerical code for extended Boussinesq equations. *ASCE Journal of Waterway*, *Port*, *Coastal*, *and Ocean Engineering* 1995; **121**(5):251–261.
14. Zang J, Lawson J, Tozer N, Dodd N. The development of a computational wave model based on extended Boussinesq equations. *Technical Report*, HR Wallingford, 1996.
15. Skotner C, Apelt CJ. Internal wave generation in an improved two-dimensional Boussinesq model. *Ocean Engineering* 1999; **26**(4):287–324.
16. Schröter A, Mayerle R, Zielke W. *Optimized Dispersion Characteristics of the Boussinesq Wave Equations*. Institute of Fluid Mechanics and Computer Applications in Civil Engineering, University of Hannover, 1994.
17. Shi F, Dalrymple RA, Kirby JT, Chen Q, Kennedy, A. A fully nonlinear Boussinesq model in generalized curvilinear coordinates. *Coastal Engineering* 2001; **42**:337–358.
18. Li YS, Zhan JM. Boussinesq-type model with boundary-fitted coordinate system. *ASCE Journal of Waterway*, *Port*, *Coastal*, *Ocean Engineering* 2001; **127**(3):152–160.
19. Antunes do Carmo JS, Seabra Santos FJ, Barthélemy E. Surface waves propagation in shallow water: a finite element model. *International Journal for Numerical Methods in Fluids* 1993; **16**:447–459.
20. Katopodes ND, Wu C. Computation of finite-amplitude dispersive waves. *ASCE Journal of Waterway*, *Port*, *Coastal*, *and Ocean Engineering* 1987; **113**(4):327–346.
21. Kawahara M, Cheng JY. Finite element method for Boussinesq wave analysis. *International Journal of Computational Fluid Dynamics* 1994; **2**:1–17.
22. Kato S, Takagi T, Kawahara M. A finite element analysis of Mach reflection by using the Boussinesq equation. *International Journal for Numerical Methods in Fluids* 1998; **28**(4):617–631.
23. Ambrosi D, Quartapelle L. A Taylor–Galerkin Method for simulating nonlinear dispersive water waves. *Journal of Computational Physics* 1998; **146**:546–569.
24. Langtangen HP, Pedersen G. Computational methods for weakly dispersive and nonlinear water waves. *Computer Methods in Applied Mechanics and Engineering* 1998; **160**:337–371.
25. Li YS, Liu S-X, Yu Y-X, Lai G-Z. Numerical modeling of Boussinesq equations by a finite element method. *Coastal Engineering* 1999; **37**:97–122.
26. Woo S, Liu PL-F. A Petrov–Galerkin finite element model for one-dimensional fully nonlinear and weakly dispersive wave propagation. *International Journal for Numerical Methods in Fluids* 2001; **37**:541–575.

27. Brown PN, Hindmarsh AC, Petzold LR. Using Krylov methods in the solution of large-scale differential–algebraic systems. *SIAM Journal on Scientific Computing* 1989; **15**(6):1467–1488.
28. Ursell F. The long-wave paradox in the theory of gravity waves. *Proceedings of the Cambridge Philosophical Society* 1953; **49**:685–694.
29. Walkley M. A numerical method for extended Boussinesq shallow-water wave equations. *Ph.D. Thesis*, School of Computer Studies, University of Leeds, U.K. 1999.
30. Zienkiewicz OC, Morgan K. *Finite Elements and Approximation*. Wiley/Interscience: New York, 1983.
31. Israeli M, Orszag SA. Approximation of radiation boundary conditions. *Journal of Computational Physics* 1981; **42**:115–135.
32. Engelman MS, Sani RL, Gresho PM. The implementation of normal and/or tangential boundary conditions in finite element codes for incompressible fluid flow. *International Journal for Numerical Methods in Fluids* 1982; **2**:225–238.
33. Kirby JT, Wei G, Chen Q, Kennedy AB, Dalrymple RA. FUNWAVE1.0 fully nonlinear Boussinesq wave model documentation and user's manual. *Technical Report CACR*-98-06, Centre for Applied Coastal Research, Department of Civil Engineering, University of Delaware, 1998.
34. Lawson J, Berzins M, Dew PM. Balancing space and time errors in the method of lines for parabolic equations. *SIAM Journal on Scientific and Statistical Computing* 1991; **12**(3):573–594.
35. Saad Y. *Iterative Methods for Sparse Linear Systems*. PWS Publishing, Boston, MA, 1996.
36. George A, Liu JW-H. *Computer Solution of Large Sparse Positive Definite Systems*. Prentice-Hall: Englewood Cliffs, NJ, 1981.
37. Benzi M, Szyld DB, Van Duin A. Orderings for incomplete factorization preconditioning of nonsymmetric problems. *SIAM Journal on Scientific Computing* 1999; **20**(5):1652–1670.
38. Brown PN, Hindmarsh AC, Petzold LR. Consistent initial condition calculation for differential–algebraic systems. *SIAM Journal on Scientific Computing* 1998; **19**(5):1495–1512.
39. Shewchuk JR. Triangle: engineering a 2D quality mesh generator and Delaunay triangulator. In Ming LC, Manocha D (eds.). *Applied Computational Geometry*. Springer: New York, 1996; 203–222.
40. Wei G, Kirby JT, Sinha A. Generation of waves in Boussinesq models using a source function approach. *Coastal Engineering* 1999; **36**:271–299.
41. Beresford PJ. Pittenweem Harbour, Fife, Scotland. Random wave disturbance studies of a proposed fishing harbour development. *Technical Report EX* 1505, HR Wallingford, 1996.
42. Larsen J, Dancy H. Open boundaries in short wave simulations—a new approach. *Coastal Engineering* 1983; **7**:285–297.